

Straight Skeletons by Means of Voronoi Diagrams Under Polyhedral Distance Functions

Stefan Huber*

Oswin Aichholzer†

Thomas Hackl†

Birgit Vogtenhuber†

Abstract

We consider the question under which circumstances the straight skeleton and the Voronoi diagram of a given input shape coincide. More precisely, we investigate convex distance functions that stem from centrally symmetric convex polyhedra as unit balls and derive sufficient and necessary conditions for input shapes in order to obtain identical straight skeletons and Voronoi diagrams with respect to this distance function.

This allows us to present a new approach for generalizing straight skeletons by means of Voronoi diagrams, so that the straight skeleton changes continuously when vertices of the input shape are dislocated, that is, no discontinuous changes as in the Euclidean straight skeleton occur.

1 Introduction

Straight skeletons and Voronoi diagrams are two prominent examples of so-called skeleton structures of shapes. Roughly speaking, a skeleton structure of a shape in \mathbb{R}^d is a $(d - 1)$ -dimensional contraction of this shape that captures certain topological and geometric features of the shape.

Though the first roots can be traced back to an article of Peschka on roof design in 1877 [11], straight skeletons were introduced to computational geometry by Aichholzer et al. [1] in the mid 90s. Given a polygon P in \mathbb{R}^2 , possibly with holes, they considered a wavefront propagation process where all edges of P move inwards in parallel and with unit speed. At any time t the wavefront $\mathcal{W}_S(t)$ forms a mitered offset of P . Over time the wavefront undergoes structural changes: Edges may shrink to length zero and vanish, or edges may be split by hitting reflex vertices. The straight skeleton $\mathcal{S}(P)$ of P is the set of loci that are traced out by the wavefront vertices, see Figure 1. Later this concept was generalized to planar straight-line graphs as input [2] and to polyhedra in three-space [3, 4, 5].

It was shown [2] that the straight skeleton cannot be interpreted as an abstract Voronoi diagram in the frame-

work of Klein [10]. In particular, the straight skeleton does not constitute a Voronoi diagram under some appropriate distance function. In this sense, straight skeletons and Voronoi diagrams are in general fundamentally different. For instance, computing straight skeletons of polygons with holes is P -complete [9], but computing Voronoi diagrams is not. Straight skeletons can change discontinuously when input vertices are moved [6], but the Voronoi diagram does not.

Under these circumstances, it is most interesting that for rectilinear input in general position (that is, a rectilinear polygon where no two edges are collinear) the straight skeleton and the Voronoi diagram under L^∞ -metric indeed coincide [2]. Barequet et al. [5] carried over this fact to rectilinear polyhedra in three-space. Furthermore, Tănase and Veltkamp [12] showed that the straight skeleton of polygons approximates the Voronoi diagram under L^2 -metric if each reflex vertex of the polygon is replaced by a particular polygonal approximation of a circular arc of infinitesimal size.

1.1 Our contribution

In this paper, we shed further light on the question under which circumstances the straight skeleton and the Voronoi diagram coincide. We consider convex distance functions that stem from appropriate convex polyhedra as unit balls and investigate necessary conditions for (an approximation of) an input shape in order to have an identical straight skeleton and Voronoi diagram under this distance function. We will see that prior results for the L^2 - and L^∞ -metric constitute the extremal cases of our general approach.

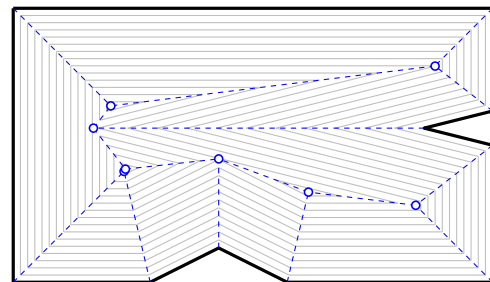


Figure 1: The straight skeleton (dashed) of a simple polygon (bold) and a couple of mitered offsets (thin).

*Institute of Science and Technology Austria, 3400 Klosterneuburg, Austria. stefan.huber@ist.ac.at

†Institute for Software Technology, Graz University of Technology, 8010 Graz, Austria. {oaich, thackl, bvogt}@ist.tugraz.at

Motivation for investigating this question is manifold. First of all, Voronoi diagrams tend to be easier to compute than straight skeletons while straight skeletons are sometimes preferred over Voronoi diagrams since they comprise only straight-line segments and no parabolic arcs. In particular, Klein presented a time-optimal $O(n \log n)$ algorithm for abstract Voronoi diagrams in the plane and several other time-optimal algorithms are known for specialized settings [10]. For straight skeletons of polygons with holes, on the other hand, there is a gap between the best known lower bound of $\Omega(n \log n)$ [8] and the currently fastest deterministic algorithm by Eppstein and Erickson [6] with a worst-case time complexity of $O(n^{17/11+\epsilon})$. Hence, Voronoi diagrams under certain polyhedral distance functions provide a more efficient access to straight skeletons.

Second, while the definition of Voronoi diagrams is naturally generalized to higher dimensions, defining straight skeletons of polyhedra turns out to be non-trivial and ambiguous. For $d = 3$, Barequet et al. [5] explicitly explain sources of ambiguity and propose a construction for (one possibility of) a valid straight skeleton. Aurenhammer and Walzl [4, 3] present an approach for generating all possible solutions, as well as an algorithm for a straight skeleton with certain special properties. For $d > 3$, no definitions have been presented so far. Using our approach, we can transfer both, the unambiguous definition and the algorithms of Voronoi diagrams, to straight skeletons for certain polyhedra.

2 Voronoi diagrams by means of wavefronts

In contrast to the straight skeleton, the Voronoi diagram is typically defined by means of a distance function f : Given a finite set S of *input sites* in d -dimensional space \mathbb{R}^d , the *Voronoi region* $\mathcal{R}(s, S)$ of $s \in S$ is defined as the set of loci that are at least as close to s as to all other $s' \in S$. The *Voronoi diagram* $\mathcal{V}(S)$ of the input sites S is then defined as the union of the boundaries of the Voronoi regions. When we speak of the Voronoi diagram $\mathcal{V}(P)$ of a polyhedron P (with holes) then we interpret the vertices, edges, and higher-dimensional faces of ∂P as the set of input sites. Hence, $\mathcal{V}(P)$ tessellates the interior of P into Voronoi regions, and each region comprises those loci that are closer to a particular face of P than to all others, see Figure 2.

Note that the above definition misses some details, especially when considering arbitrary convex distance functions and degeneracies in the input polyhedra. For a precise definition (of the skeleton) of $\mathcal{V}(P)$, special care needs to be taken in order to avoid faces of $\mathcal{V}(P)$ to possess non-zero measure. See for instance the concept of “cone of influence” in [7].

To avoid the discussion of these technical details, we interpret the Voronoi diagram as the interference pat-

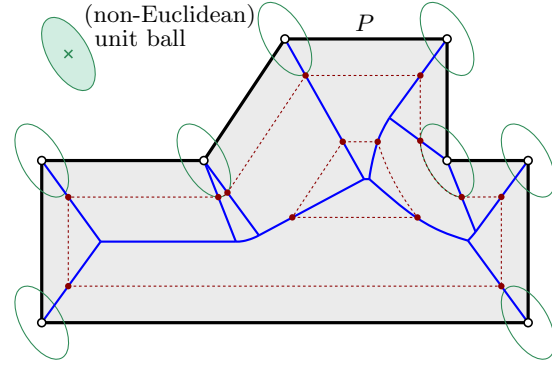


Figure 2: The Voronoi diagram $\mathcal{V}(P)$ of the polygon P . The distance function is induced by the given unit ball. P is tessellated into Voronoi regions. Two Minkowski offsets are shown in red. $\mathcal{V}(P)$ is the interference pattern of the wavefront forming Minkowski offsets.

tern of a wavefront process, similar to the one of the straight skeleton. But while straight skeletons are based on mitered offsets, Voronoi diagrams are related to offsets based on the Minkowski sum. For two non-empty sets X and Y in a vector space, the *Minkowski sum* $X \oplus Y$ is defined as the set $\{x + y : x \in X, y \in Y\}$. The *Minkowski difference* $X \ominus Y$ is then defined as $\{z \in \mathbb{R}^d : \{z\} \oplus Y \subseteq X\}$, which is, roughly speaking, the largest set whose Minkowski-sum with Y still fits into X . That is, $(X \ominus Y) \oplus Y \subseteq X$, and if Y contains the origin o , then $X \ominus Y \subseteq X$.

For the remainder of this paper, we assume that the convex distance function f is induced by a norm $\|\cdot\|$ on \mathbb{R}^d , i.e., for all $x, y \in \mathbb{R}^d$ it holds that $f(x, y) = \|x - y\|$. This allows us to define by $B := \{x \in \mathbb{R}^d : \|x\| \leq 1\}$ the *unit ball* of the normed vector space $(\mathbb{R}^d, \|\cdot\|)$. It is easy to see that a unit ball is a compact, centrally symmetric, convex set. We define the *Minkowski offset* $\mathcal{W}_{\mathcal{V}}(t)$ at time $t \geq 0$ by $\partial(P \ominus t \cdot B)$, that is, as the boundary of the Minkowski difference of P with the unit ball scaled by t . Since B is o -symmetric, i.e., $B = -B$, we obtain

$$\mathcal{W}_{\mathcal{V}}(t) = P \cap \partial(\partial P \oplus t \cdot B). \quad (1)$$

The Minkowski offset $\mathcal{W}_{\mathcal{V}}$ of P and the Voronoi diagram $\mathcal{V}(P)$ of P are in an intimate relationship: Any point p of $\mathcal{W}_{\mathcal{V}}(t)$ is in the Voronoi region of some face s of P . Moreover, p has infimum distance t to ∂P , and as p lies in the Voronoi region $\mathcal{R}(s, P)$ of $s \subset \partial P$, this distance is attained at a point of s . Plugging this observation into (1), we can construct $\mathcal{W}_{\mathcal{V}}(t)$ within each Voronoi region of $\mathcal{V}(P)$ independently:

$$\mathcal{W}_{\mathcal{V}}(t) = P \cap \bigcup_{\text{face } s \text{ of } \partial P} \mathcal{R}(s, P) \cap \partial(s \oplus t \cdot B). \quad (2)$$

On points of the Voronoi diagram — that is, on the boundaries of Voronoi regions — the Minkowski offsets

of two different faces of ∂P interfere. In this sense, we can interpret the Voronoi diagram $\mathcal{V}(P)$ as the interference pattern of Minkowski offsets, see again Figure 2.

With this interpretation of the Voronoi diagram, the above mentioned technical details would be needed for precisely defining the interference patterns of the Minkowski offset. However, for the purpose of our work, which is comparing the straight skeleton of a polyhedron with its Voronoi diagram, it is sufficient to compare their respective wavefronts. Therefore, we will consider the Minkowski offsets instead of the (actual) Voronoi diagram for the remainder of this paper.

3 Proper unit balls and input shapes

The aim of our paper is to investigate when the Voronoi diagram w.r.t. some distance function is equal to the straight skeleton. The distance function is induced by a norm, and the norm, on the other hand, can be specified by the unit ball B , i.e., $\|x\|_B = \inf\{t \geq 0 : x \in tB\}$. Together with the interpretation of Voronoi diagrams from the previous section, we can rephrase our main question as follows:

For which unit balls and for which input shapes is the Minkowski offset $\mathcal{W}_V(t)$ equal to the mitered offset $\mathcal{W}_S(t)$ for all $t \geq 0$?

3.1 Proper unit balls

As B is the unit ball corresponding to a convex distance function, B has to be convex and o -symmetric.

The wavefront $\mathcal{W}_S(t)$ at any time t has a piecewise linear geometry. Each of its facets are parallel and at distance t to one of the facets of the input polyhedron P . In general, the Minkowski offset of P comprises features of ∂P and ∂B . Hence, B needs to be polyhedral in order for the Minkowski offset to be polyhedral for all polyhedra P .¹

Furthermore, at least for the most basic polyhedron P , namely $P = B$, the Minkowski and mitered offsets should be equal. Note that $P = B$ implies $\mathcal{W}_V(t) = (1-t) \cdot B$. At $t = 1$ the wavefront collapsed to a point at the origin o . In two dimensions, $\mathcal{V}(P)$ forms a star graph with a single vertex at o and each edge e of P has a triangle spanned by e and o as Voronoi region. In higher dimensions, the Voronoi region of each facet s is given by the convex hull spanned by o and s . On the other hand, the facets of the wavefront $\mathcal{W}_S(t)$ all move at unit speed. In order for $\mathcal{W}_S(t) = \mathcal{W}_V(t)$ to

¹For convex polyhedra P , the Minkowski offset of P would be polyhedral even if ∂B is a smooth surface. In particular, it is known that $\mathcal{S}(P) = \mathcal{V}(P)$ w.r.t. the L^2 -norm for convex polyhedra P . In fact, it is possible that B is only piecewise polyhedral and the Minkowski offset of P would still be polyhedral for certain non-convex polyhedra P . However, for the sake of simplicity, we assume for this paper that B is polyhedral.

hold, the facets of B need to have unit distance to o . In other words, the Euclidean unit ball centered at o is tangential to all facets of B . We say that B is *isotropic* if all facets have unit distance to the origin.²

Definition 1 *A proper unit ball is a convex, isotropic, o -symmetric polyhedron.*

Lemma 1 *For a proper unit ball B and any $v \in \mathbb{R}^d$ it holds that $\|v\|_2 \geq \|v\|_B$, and equality holds exactly when v is a normal vector of a facet of B .*

Proof. The inequality holds as the Euclidean unit ball O is contained in B . Furthermore, $\|v\|_2 = \|v\|_B$ holds for exactly those v for which $v/\|v\|_B \in \partial B \cap \partial O$, i.e., where $v/\|v\|_B$ is a contact point of a facet of B with the boundary of O . \square

3.2 Proper input shapes

For the remainder of this paper, let B denote a proper unit ball. In the following, we will investigate necessary conditions for a polyhedral input shape P such that the Minkowski offset and mitered offset are equal. A restriction to connected sets is not essential, as we can consider each component independently. We will denote by P an input shape in the following sense.

Definition 2 *A (d -dimensional) input shape P is a connected, compact set in \mathbb{R}^d whose boundary forms a polyhedral surface that constitutes an orientable $(d-1)$ -manifold.*

Denote by $\text{relint}_A(X)$ the relative interior of X w.r.t. A , i.e., the interior of X in the subspace topology on A . Furthermore, let $\text{relint } X$ be a shorthand notation for $\text{relint}_{\text{aff}(X)} X$, where $\text{aff}(X)$ is the affine hull of X .

Definition 3 *A face f of P of dimension at most $d-2$ is called reflex if for any point $p \in \text{relint } f$ and for any Euclidean ball O that is centered at p and has sufficiently small but positive radius, $O \setminus P$ is contained in a half-space whose boundary supports p .*

In order for the facets of the wavefronts of \mathcal{W}_V and \mathcal{W}_S to propagate at the same speed, it follows from Lemma 1 that the orientations of the facets correspond to orientations of facets of B . We denote by $n(f)$ the normal vector of the facet f of P pointing to the interior.

Lemma 2 *Every facet f of P has a corresponding facet f^B of B that has $n(f)$ as the outer normal vector, unless $\mathcal{W}_V(\varepsilon) \neq \mathcal{W}_S(\varepsilon)$ for some $\varepsilon > 0$.*

²By considering weighted straight skeletons, one could assign the facet's distance to o as weight. Hence, each wavefront's facet would again reach o at time 1.

Proof. Let p be a point in relint f . For a sufficiently small $\varepsilon > 0$, the point $p' = p + \varepsilon n(f)$ is in the relative interior of the facet of $\mathcal{W}_S(\varepsilon)$ emanated by f . Assuming that $\mathcal{W}_S(\varepsilon) = \mathcal{W}_V(\varepsilon)$, p' is also in the relative interior of the same facet of $\mathcal{W}_V(\varepsilon)$ and, thereby, $\|p - p'\|_B = \varepsilon$. By Lemma 1, $n(f)$ is a normal vector of a facet of B . \square

3.2.1 Two-dimensional input shapes

Let us assume that $d = 2$, i.e., P is a polygon with zero or more holes. Lemma 2 tells us that for any edge e of P there is an edge e^B of B whose normal vectors match if the wavefronts \mathcal{W}_S and \mathcal{W}_V are equal. The following lemma states that, in addition, P and B look locally the same at reflex vertices of P .

Lemma 3 *Let v be a reflex vertex of P with incident edges e_1 and e_2 . Then there is a corresponding vertex v^B of B that is incident to e_1^B and e_2^B , unless $\mathcal{W}_V(\varepsilon) \neq \mathcal{W}_S(\varepsilon)$ for some $\varepsilon > 0$.*

Proof. For a sufficiently small $\varepsilon > 0$, the two edges e'_1 and e'_2 of $\mathcal{W}_S(\varepsilon)$, which were emanated from e_1 and e_2 respectively, are incident to a vertex v' of $\mathcal{W}_S(\varepsilon)$. By $\mathcal{W}_S(\varepsilon) = \mathcal{W}_V(\varepsilon)$, we have $\|v' - v\|_B = \varepsilon$. Hence, the point $v^B = (v' - v)/\varepsilon$ lies on ∂B , is incident to e_1^B and e_2^B , and, thereby, is a vertex of B . \square

It turns out that the two necessary conditions for $\mathcal{W}_S(\varepsilon) = \mathcal{W}_V(\varepsilon)$ collected by Lemma 2 and Lemma 3 are also sufficient, see Theorem 5 below. This motivates the following definition.

Definition 4 *A proper input shape P w.r.t. a proper unit ball B in \mathbb{R}^2 is a polygon with holes such that*

- (I1) *for each edge e of P there is a corresponding edge e^B of B whose outer normal vector is $n(e)$ and*
- (I2) *for each reflex vertex v of P , incident to edges e_1 and e_2 , there is a corresponding vertex v^B of B that is incident to e_1^B and e_2^B .*

We can distinguish between three different events that can happen during the wavefront propagation: the so called vertex, edge, and split events. For details see for instance [8]. In the following lemma we prove that some of these events cannot arise in our setting.

Lemma 4 *For a proper input shape P w.r.t. a proper unit ball B in \mathbb{R}^2 no vertex events happen for \mathcal{W}_S . Further, no split events where a single reflex vertex splits a single wavefront edge into two, happen for \mathcal{W}_S .*

Proof. We first prove that no vertex event can happen, i.e., no new reflex wavefront vertex is created because two (or more) reflex vertices meet, see Figure 3 (a). Assume to the contrary that a vertex event happens at

some time t and the new reflex wavefront vertex is incident to edges e_1 and e . Then e_1 and another edge e_2 were incident to a reflex vertex just before time t . W.l.o.g. we assume that the clockwise-angle between $n(e_1)$ and $n(e_2)$ is less than π . By (I2) in Definition 4, there would be no edge of B whose normal vector is between $n(e_1)$ and $n(e_2)$ in clockwise direction, but $n(e)$ is, which is a contradiction and proves the first statement.

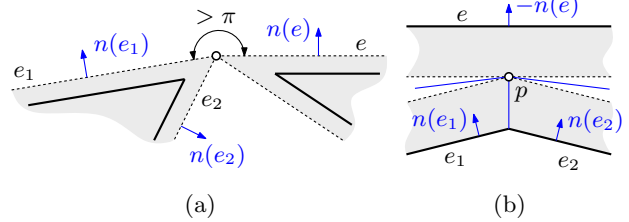


Figure 3: Two events violating (I2) in Definition 4. (a) A vertex event. (b) A split event, where a reflex wavefront vertex meets a single edge that is split into two.

To prove the second statement assume that a single reflex vertex between edges e_1 and e_2 meets and splits a single wavefront edge e into two, see Figure 3 (b). We again assume w.l.o.g. that the clockwise angle between $n(e_1)$ and $n(e_2)$ is less than π . By the symmetry of B , $-n(e)$ is a normal vector of an edge of B . Again, (I2) in Definition 4 is violated as $-n(e)$ lies between $n(e_1)$ and $n(e_2)$ in clockwise order. \square

Theorem 5 *Let B be a proper unit ball B and P be an input shape in \mathbb{R}^2 . Then $\mathcal{W}_S(t) = \mathcal{W}_V(t)$ for all $t \geq 0$ if and only if P is proper.*

Proof. If $\mathcal{W}_S(t) = \mathcal{W}_V(t)$ for all $t \geq 0$, then P is proper by Lemma 2 and Lemma 3. Let us now prove the converse. We first show that both wavefronts are equal until the first (edge or split) event. Then we prove that each event causes the same structural change to either wavefront. Hence, by induction, the wavefronts are equal at all times.

Note that due to (I1) in Definition 4 the wavefront edges in \mathcal{W}_S and \mathcal{W}_V start to propagate at equal speeds. For all sufficiently small $\varepsilon > 0$, each vertex and edge of $\mathcal{W}_S(\varepsilon)$ is emanated from exactly one vertex and edge of P , and hence P and $\mathcal{W}_S(\varepsilon)$ are combinatorially equal by definition of straight skeletons. The same holds for $\mathcal{W}_V(\varepsilon)$ for all edges and convex vertices and due to (I2) in Definition 4 also for reflex vertices. Hence, $\mathcal{W}_S(\varepsilon) = \mathcal{W}_V(\varepsilon)$ for all sufficiently small $\varepsilon > 0$. Both wavefronts propagate continuously as their vertices move at constant speed. Therefore, at least until the first event both wavefronts are equal.

Assume that an event happens at some fixed time t and $\mathcal{W}_S(t - \varepsilon) = \mathcal{W}_V(t - \varepsilon)$ for all $\varepsilon \geq 0$. By Lemma 4 this event is neither a vertex event nor a split event,

where a single reflex vertex meets and splits a single wavefront edge e into two.

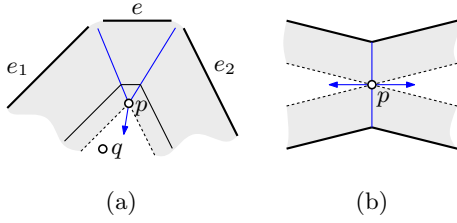


Figure 4: (a) Edge and (b) split events cause the same structural transformations for \mathcal{W}_S and \mathcal{W}_V .

Let us assume that an edge event happened at point p when the edge e collapsed and the edges e_1 and e_2 become adjacent in \mathcal{W}_S , see Figure 4 (a). We denote by $b(e_i, e_j)$ the bisector between two edges e_i and e_j . Two straight-skeleton edges on the bisectors $b(e, e_1)$ and $b(e, e_2)$, respectively, end at p and a new one on $b(e_1, e_2)$ originates. In \mathcal{W}_S the wavefront is locally modified by removing edge e and making e_1, e_2 adjacent. We show that \mathcal{W}_V undergoes the same structural change locally at p . Let q be any point locally at p that was not yet swept by the wavefront. Note that q lies at the side of e_1 w.r.t. $b(e_1, e)$ or at the side of e_2 w.r.t. $b(e_2, e)$. Hence, q is closer to e_1 or e_2 than to e with respect to B after the event. More specifically, locally at p any point of \mathcal{W}_S after the event is closer to e_1 or e_2 than to e . By a similar analysis it can be seen that split events transform \mathcal{W}_S and \mathcal{W}_V in the same way, see Figure 4 (b). \square

Note that unlike Voronoi diagrams, the straight skeleton of a polygon may change discontinuously when vertices of the polygon are dislocated [6, 8]. However, this can only happen at the presence of vertex events. By Theorem 5, the straight skeleton of proper input shapes changes continuously as the Voronoi diagram does, and Lemma 4 tells us why.

3.2.2 Higher-dimensional input shapes

Let P denote an input shape in \mathbb{R}^d for any $d \geq 2$. In the two-dimensional setting, we observed that at non-convex locations of the input shape, the input shape locally looks the same as the unit ball, in order for the wavefronts to be equal. For dimensions greater than two, we make the same general observation. However, since there is a much larger diversity of non-convexity in dimension three or higher, the situation becomes significantly more complicated. For instance, for $d = 3$ a vertex may be neither convex nor reflex, but constitute a saddle point. Furthermore, both convex and reflex edges may be incident to a convex (or reflex) vertex.

Nevertheless, an edge e of an input shape \mathbb{R}^3 is either convex or reflex, as the two incident faces form either an interior angle of $\leq \pi$ or $> \pi$. In fact, for

arbitrary dimensions $d \geq 2$, the $(d - 2)$ -dimensional faces are incident to exactly two facets as ∂P forms a $(d - 1)$ -manifold. This observation enables us to generalize Lemma 3 to arbitrary dimension:

Lemma 6 *Let P be an input shape in \mathbb{R}^d , where $d \geq 2$. For each reflex $(d - 2)$ -dimensional face e of P , which is incident to facets f_1 and f_2 , it holds that $f_1^B \cap f_2^B \neq \emptyset$, unless $\mathcal{W}_V(\varepsilon) \neq \mathcal{W}_S(\varepsilon)$ for some $\varepsilon > 0$.*

Proof. The case $d = 2$ is established by Lemma 3. Assume that $d \geq 3$ and consider a point p in the relative interior of e . The affine hull $\text{aff}(e)$ of e can be depicted as $p + H$, where H is a $(d - 2)$ -dimensional vector space. Let us denote by H^\perp the orthogonal complement of H , which is of dimension 2.

By $\text{aff}(e) \subset \text{aff}(f_1)$ it follows that $\text{aff}(f_1) \cap (p + H^\perp)$ is a 1-dimensional affine sub-space. Hence, $f_1 \cap (p + H^\perp)$ forms a line-segment that is incident to p , and the same holds for $f_2 \cap (p + H^\perp)$. As $n(f_1), n(f_2) \perp \text{aff}(e)$ it follows that $n(f_1), n(f_2) \in H^\perp$. This means that also the intersections of the facets of the wavefront with $p + H^\perp$ constitute line segments that move at unit speed within H^\perp w.r.t. Euclidean metric and w.r.t. $B \cap H^\perp$. This allows us to reduce the problem to the two-dimensional case within $p + H^\perp$. By a similar argument as in Lemma 3 we see that $f_1^B \cap H^\perp$ and $f_2^B \cap H^\perp$ have a point in common, and so have f_1^B and f_2^B . \square

Note that from $f_1^B \cap f_2^B \neq \emptyset$ it does not necessarily follow that the face $f_1^B \cap f_2^B$ of B is $(d - 2)$ -dimensional. That is, roughly speaking, the face e of the last lemma might not have a corresponding face e^B in B . In fact, a polyhedron P and a proper unit ball B exist in \mathbb{R}^3 such that both wavefronts are equal at all times, but still P contains a reflex edge incident to two facets whose corresponding facets do not form an edge of B .

Definition 5 *An input shape P in \mathbb{R}^d is called proper w.r.t. a proper unit ball B if*

- (I1) *for each facet f of P there is a corresponding facet f^B of B whose outer normal vector is $n(f)$ and*
- (I2) *for all points p on all facets f of P , there is a point p' such that $\inf_{q \in P} \|p' - q\|_B = \|p' - p\|_B > 0$ and $p \in \text{relint}_f(f \cap (p' + \|p' - p\|_B \partial B))$.*

Note that in the above definition condition (I1) is implied by condition (I2). We chose to state both conditions nevertheless, to illustrate the similarity to Definition 4. In fact, for $d = 2$ Definition 4 and Definition 5 agree as the condition (I2) of the latter is equivalent to conditions (I1) and (I2) of the former.

The intuitive interpretation of this definition is the following: to any point p on the surface of a proper input shape P one can always attach a sufficiently small

unit ball B from outside that has an intersection with ∂P with non-empty relative interior. If ∂P is locally convex at p , then this is a trivial statement.

Lemma 7 *For any $0 < \varepsilon < 1$, one can depict B as the union of finitely many translates of εB .*

Proof. We can place at each vertex of B a translate of μB such that this translate is contained in B and covers the vertex. By setting $\mu \geq 1/2$, every point within B is covered by one translate. By setting $\mu \leq 1$, the translates stay within B . By repeating this method at most $(-\log_2 \varepsilon)$ times, we obtain finitely many translates of εB that cover B . \square

Lemma 8 *For any proper input shape P w.r.t. B there is a finite point set S and some $\varepsilon > 0$ such that $\partial P \subseteq \partial(S \oplus \varepsilon B)$.*

Proof. (Sketch) Let us consider a facet f of P . For every point $p \in f$ we consider its point p' according to (I2). Let us endow f with the relative topology from \mathbb{R}^d . Then the sets $\text{relint}_f(f \cap (p' + \|p' - p\|_B \partial B))$ yield an open cover of the compact space f . Hence, there is a finite sub-cover, and thus a finite point set S such that

$$\partial P \subset \partial \bigcup_{p' \in S} p' + \left(\inf_{q \in P} \|p' - q\|_B \right) B.$$

Let us set $\varepsilon = \min_{p'} \inf_{q \in P} \|p' - q\|_B$. By Lemma 7 we can replace each $(\inf_{q \in P} \|p' - q\|_B) B$ by finitely many translates of εB . \square

The last lemma allows us to see the wavefront \mathcal{W}_γ as the wavefront that started from a finite point set S . For sufficiently small t , the set $S \oplus tB$ consists of disjoint translates of scaled unit balls. As balls grow they start to merge and at time $t = \varepsilon$ the set $S \oplus tB$ tightly encloses P in the sense that $\partial P \subset (S \oplus \varepsilon B)$.

Note that $S \oplus \varepsilon B$ plays the role of the complement of P and, thereby, reflex features of P are convex features of $S \oplus \varepsilon B$. During the growth of $S \oplus tB$ the convex features do not change orientation and no convex features with new orientations are introduced. That means:

Lemma 9 *Locally at reflex faces proper input shapes P look the same as B .*

We will give formal details in the full version of this paper.

The intention of our argumentation until this point was to show that the wavefronts of the straight skeleton and the Voronoi diagram coincide for a proper input shape w.r.t. a proper unit ball. Therefore the wavefront of the straight skeleton is uniquely defined for this special setting. We conclude with the following theorem which can also be considered as a definition for straight skeletons of proper input shapes in dimension three and higher.

Theorem 10 *For a proper input shape P w.r.t. a proper unit ball B in \mathbb{R}^d it holds that $\mathcal{W}_S(t) = \mathcal{W}_\gamma(t)$ for all $t \geq 0$.*

Let us finally remark that any given shape can be approximated by a proper input shape. This can be achieved by standard approximation techniques. Details will be presented in the full version of this work.

4 Conclusion

In this paper we presented a new approach for generalizing straight skeletons by means of Voronoi diagrams. All previous approaches have common constitutive principles, which are also fulfilled by our approach: (i) All facets of the wavefront \mathcal{W}_γ are parallel copies of facets of P that move at unit speed. (ii) No facet of \mathcal{W}_γ is emanated from a face of a facet, i.e., every facet of \mathcal{W}_γ was emanated by a facet of P , cf. Lemma 9.

Our presented combination of proper unit balls and corresponding proper input shapes ensures that the straight skeleton and the Voronoi diagram essentially coincide. This concept is stated in Theorem 10. For $d = 2$, where the straight skeleton is thoroughly defined, this fact is proven in Theorem 5. For $d = 3$, different approaches already exist to transfer the concept of straight skeletons to three-space. Due to lack of space we adjourn a detailed comparison to a full length version of this work. For $d > 3$, there is no prior work that aims to define straight skeletons. Hence, for this case Theorem 10 could be read as a definition for straight skeletons for a proper setting.

References

- [1] O. Aichholzer, D. Albers, F. Aurenhammer, and B. Gärtner. A novel type of skeleton for polygons. *Journal of Universal Computer Science*, 1(12):752–761, Dec. 1995.
- [2] O. Aichholzer and F. Aurenhammer. Straight skeletons for general polygonal figures in the plane. In A. Samoilenko, editor, *Voronoi's Impact on Modern Science, Book 2*, pages 7–21. Institute of Mathematics of the National Academy of Sciences of Ukraine, Kiev, Ukraine, 1998.
- [3] F. Aurenhammer and G. Walzl. Structure and computation of straight skeletons in 3-space. In *Lecture Notes in Computer Science (LNCS), Proc. 24th International Symposium on Algorithms and Computation (ISAAC 2013)*, pages 44–54, Hong Kong, 2013.
- [4] F. Aurenhammer and G. Walzl. Three-dimensional straight skeletons from bisector graphs. In *Proc. 5th International Conference on Analytic Number Theory and Spatial Tessellations*, pages 58–59, Kiev, Ukraine, 2013.
- [5] G. Barequet, D. Eppstein, M. T. Goodrich, and A. Vaxman. Straight skeletons of three-dimensional polyhedra.

In *Lecture Notes in Computer Science (LNCS), Proc. 16th European Symposium on Algorithms (ESA 2008)*, volume 5193, pages 148–160, 2008.

- [6] D. Eppstein and J. Erickson. Raising roofs, crashing cycles, and playing pool: Applications of a data structure for finding pairwise interactions. *Discrete & Computational Geometry*, 22(4):569–592, 1999.
- [7] M. Held and S. Huber. Topology-oriented incremental computation of Voronoi diagrams of circular arcs and straight-line segments. *Computer-Aided Design*, 41(5):327–338, May 2009.
- [8] S. Huber. *Computing Straight Skeletons and Motorcycle Graphs: Theory and Practice*. Shaker Verlag, Apr. 2012. ISBN 978-3-8440-0938-5.
- [9] S. Huber and M. Held. Approximating a motorcycle graph by a straight skeleton. In *Proc. 23rd Annual Canadian Conference on Computational Geometry (CCCG '11)*, pages 261–266, Toronto, Canada, Aug. 2011.
- [10] R. Klein, E. Langetepe, and Z. Nilforoushan. Abstract voronoi diagrams revisited. *Computational Geometry: Theory and Applications*, 42(9):885–902, Nov. 2009.
- [11] G. A. Peschka. *Kotierte Ebenen und deren Anwendungen*. Verlag Buschak & Irrgang, Brünn, 1877.
- [12] M. Tănase and R. C. Veltkamp. A straight skeleton approximating the medial axis. In *Lecture Notes in Computer Science (LNCS), Proc. 12th European Symposium on Algorithms (ESA 2004)*, pages 809–821, Sept. 2004.